MPC-Controlled Virtual Synchronous Generator to Enhance Frequency and Voltage Dynamic Performance in Islanded Microgrids

Long, Bo; Liao, Yong; Chong, Kil To; Rodríguez, José; Guerrero, Josep M.

Published in:
IEEE Transactions on Smart Grid

DOI (link to publication from Publisher):
10.1109/TSG.2020.3027051

Publication date:
2021

Document Version
Accepted author manuscript, peer reviewed version

MPC-Controlled Virtual Synchronous Generator to Enhance Frequency and Voltage Dynamic Performance in Islanded Microgrids

Bo Long, *Member, IEEE,* Yong Liao, *Student Member, IEEE,* Kil To Chong, Jose Rodriguez, *Fellow, IEEE, and Josep M. Guerrero*

***Abstract*—The use of high penetration converter-interfaced renewable energy (RE) based microgrids (MGs), due to the absence of rotational masses from conventional synchronous generators (SGs), may lead to a lack of inertia, which may lead the steeper frequency and voltage fluctuations that may in turn cause instability issues and challenges the normal operation of sensitive loads. To suppress these fluctuations and enhance the MGs stability, a novel model predictive control (MPC)-controlled virtual synchronous generator (VSG) for an energy storage system (ESS) is introduced. The proposed method can provide inertia support during transient states and enhance the dynamic characteristics of system voltage and frequency. By establishing the prediction model of VSG and designing the cost function for frequency and power, the increments of the needed active and reactive power are calculated then superposed on the power reference of VSG. The results show that the suppression performance of the voltage and frequency variations under loading transition with the proposed method is better than those of other techniques. Simulation and hardware-in-the-loop (HIL) results further demonstrate the effectiveness of the proposed method.**

***Index Terms*—Renewable energy (RE), energy storage system (ESS), model predictive control (MPC), virtual synchronous generator (VSG).**

I. Introduction

FREQUENCY fluctuations are more likely to occur in high penetration solar and wind energy microgrids (MGs) because MGs containing power converters lack inertial support. There are many control methods available for MGs. A general overview of existing control methods is provided in [1], where various power-sharing methods are categorized and compared. Conventional droop control, due to its effectiveness in power-sharing between multi-parallel connected power converters, has been applied in a wide variety of areas [2]. A coordinated architecture of islanded AC MGs with smooth switching droop control has been proposed in one study to provide a flexible power control [3]. Based on cooperative control techniques, some other novel controllers have been described that use local information and nearest-neighbor communication to collectively realize secondary control [4-6].

To compensate for the lack of inertia in droop control, virtual synchronous generator (VSG) control is proposed [7, 8]. Various studies have applied this VSG method is to the power converter of a distributed power generation system (DPGS) to provide active and reactive power support to maintain the system power balance and stability by mimicking the behavior of a synchronous machine [9-11]. In another study, the VSG is controlled with a droop controller along with virtual inertia introduced by a first-order low-pass filter in the power droop [12]. A VSG control method with an alternating moment of inertia has also been described to improve the performance in the fast frequency oscillations damping [13]. To enhance the frequency stability with an interleaving control technique, a self-adaptive inertia and damping combination control method has been proposed [14]. In [15], an algebraic-type VSG with minimum parameter numbers is used to suppress the system frequency and voltage deviations.

The power fluctuation suppression methods that have been reported to date can be divided into two types: those with an energy storage system (ESS) [16-18] and those without an energy storage system [19, 20]. Suppression methods without energy storage devices are much less expensive, but their performances in practice are substantially limited because they have no additional power support. In a wind power generation system, the inertia is typically produced from the rotor of the permanent magnetic synchronous generator (PMSG). The energy storage device based frequency variation suppression method can achieve better performance and ensure system stability. Moreover, it can be installed at the final point of common coupling (PCC) of MGs, making it more flexible and independent. As a result, this energy storage system has been widely used due to its mature status, and many control methods for it have been proposed [21, 22].

The latest studies on MPC control in ESS have mainly focused on coordinating the charge and discharge control of multiple ESSs through the MPC method [23, 24]. In addition, the MPC controller can also decide the current power reference based on the prediction of the required output power at the next

Manuscript received January 31, 2020; revised August 15, 2020; accepted September 23, 2020. This paper is sponsored by the Fundamental Research Funds for the Central Universities of China (NO. ZYGX2019J033), Key R & D plan of science and Technology Department of Sichuan Province (20ZDYF2816), State Key Laboratory of Control and Simulation of Power System Generation Equipment, China (SKLD20M11), Tsinghua University, China, and by the VELUX FOUNDATIONS under the VILLUM Investigator Grant Center for Research on Microgrids (CROM) (Award Ref. No.: 25920): (Corresponding Author: Bo Long.)

Bo Long and Yong Liao, are with the School of Mechanical and Electrical Engineering, University of Electronic Science and Technology of China 611731, China (e-mail:longbouestc1980@126.com;liaoyong9543@163.com).

Kil To Chong is with the Department of Electronics and Information Engineering, Jeonbuk National University, Jeonju 54896, South Korea, (e-mail: kitchong@jbnu.ac.kr).

J. Rodriguez is with the Faculty of Engineering, Universidad Andres Bello, Santiago 8370146, Chile (e-mail: jose.rodriguez@unab.cl).

Josep M. Guerrero is with the Department of Energy Technology, Aalborg University, Aalborg DK-9220, Denmark. (email: joz@et.aau.dk).

sampling period, thereby providing better power tracking performance [25]. In [26], an MPC-based plug-in hybrid electric vehicles' power control is used to alleviate the frequency fluctuation of MGs.

In islanded MGs with renewable sources, load changes, wind fluctuation, and many other types of changes can significantly influence the system frequency [27]. In [28], H_∞ and μ-synthesis approaches are used to suppress frequency fluctuations. In [29], a combination of the general Type-2 Fuzzy-Logic sets and the modified harmony search algorithm is proposed to provide better load frequency regulation capability. Sliding mode control (SMC) is also used in load frequency control [30]. Electric springs based on power electronics have also been proposed to provide active and reactive power for load changes [31]. In [32], VSG is used to improve the transient power- sharing between SG and DG in MGs.

The conventional VSG-ESS method could not achieve good dynamic frequency and voltage stabilities due to the intermittent renewable energy; if the system frequency fluctuates substantially, the regulation capability of the VSG-ESS is limited when changing only the inertia and damping coefficients. The rate-of-change-of-frequency (ROCOF) may be too large to be kept within the requirements. Therefore, in this paper, an MPC-VSG is proposed for ESS control, which can simultaneously enhance the dynamic characteristics of frequency and voltage at PCC. To begin, the mathematical model that combines MPC and VSG is derived. Then the rated power changes in the VSG are predicted by MPC, and the rated power of VSG is modified, which can improve the dynamic frequency characteristics. Meanwhile, considering that the active power changes may lead to variations in the grid voltage, the reactive power of VSG is regulated by MPC, which can reduce the grid voltage variation. In summary, the proposed MPC-VSG method has the following advantages.

1) In the conventional active-power frequency VSG control method, the reference power typically remains unchanged once initialized. It is mainly used for inertia and primary frequency regulation, which does not contribute substantially to the secondary frequency regulation. The proposed MPC-VSG method can calculate the increment power needs by solving the optimized cost function with the allowable maximal and minimal frequency variation ranges constraints according to the current status, which can reduce the frequency drift during transient states as an auxiliary aid to the diesel generator.
2) Once a disturbance occurs in MGs, the proposed MPC-VSG method can change the output power reference of VSG in consideration of the minimization of ROCOF, voltage, and frequency error, which is superior to the conventional VSG method.

This paper is organized as follows. Section II demonstrates the frequency fluctuation mechanism of parallel-connected power converter MGs with solar and wind power energy, etc. Some basic concepts of VSG are also discussed. Section Ⅲ presents the derivation of the proposed MPC-VSG ESS method, and the cost function design with output constraints and system stability are also analyzed. In Section Ⅳ and Ⅴ, the effectiveness of the proposed control method is verified through simulation and hardware-in-the-loop experimental results. Finally, Section Ⅵ concludes this paper and outlines future research directions.

II. Problem Description and VSG

A. Frequency and Voltage Fluctuations in MGs

MGs can operate in two modes: island mode and grid-connected mode [33]. When MGs are connected with an ideal grid, the PCC frequency and voltage are fully supported by the grid, so voltage-frequency fluctuations will not occur. However, when MGs operate in island mode composed of a wind turbine, photovoltaic (PV) system, loads, energy storage system, etc., as shown in Fig. 1, grid frequency-voltage fluctuations may occur since there is no ideal power support from the grid, and the MGs may face stability challenges due to the lack of inertia.

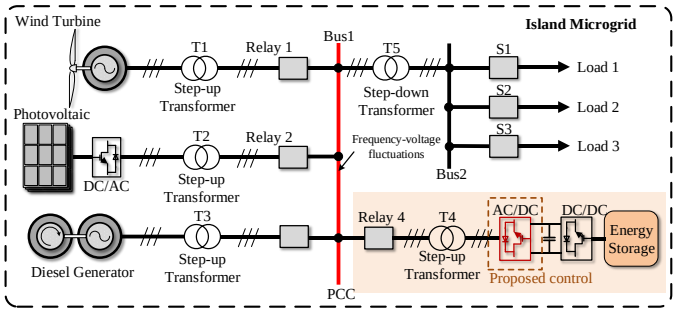

Fig. 1. Islanded microgrid system.

When MGs operate in islanded mode, all the power converters are connected in parallel to supply power to the loads, as shown in Fig. 1. A diesel generator can suppress frequency deviations with inertial forces and automatic voltage regulators (AVRs), so the frequency is mainly supported by a diesel generator. However, when the voltage-frequency of MGs is purely supported by RE, the power-electronics-based RE cannot provide sufficient inertia support. With the increased penetration of RE, the dynamic response of PCC frequency and voltage will be further degraded.

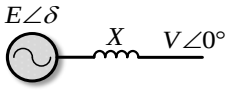

Fig. 2. Simplified synchronous generator model connected with an ideal grid.

Fig. 2 shows a simplified synchronous generator (SG) model that is connected with an ideal grid, through which, the output power of the synchronous generator can be obtained as

$$P_{SG} = \frac{EV}{X}\sin\delta,\ Q_{SG} = \frac{EV}{X}\cos\delta - \frac{V^2}{X} \tag{1}$$

Where P_{SG} and Q_{SG} are the active and reactive power output of SG, respectively; E and V are the voltages of SG and point of common coupling (PCC), respectively; X is the line inductance and δ is the power angle.

The variations of active and reactive power in SG can be derived by converting (1) to a small-signal-model as

$$\begin{cases} \Delta P_{SG} = \frac{E\Delta V}{X}\sin\delta_0 + \frac{EV_0}{X}\cos\delta_0\Delta\delta \\ \Delta Q_{SG} = \frac{E\Delta V}{X}\cos\delta_0 - \frac{2V_0\Delta V}{X} - \frac{EV_0}{X}\sin\delta_0\Delta\delta \end{cases} \quad (2)$$

where δ_0 is the power angle in steady state, and V_0 is the steady-state PCC voltage. The changes in power angle $\Delta\delta$ can indirectly indicate the system frequency f. It can be seen that f is related to the changes in active power output ΔP_{SG} and voltage output ΔV.

There are two main reasons that may lead to frequency and voltage variations in MGs, namely unstable energy from RE and load changes, which are described as follows:

In practice, wind power and solar energy output are typically not stable. When the wind speed is low, the generated wind power is also small, and vice versa. Similarly, when the illumination of the PV array changes, the generated power of the photovoltaic (PV) system may also change. As a result, this unstable and intermittent energy can also cause frequency and voltage fluctuations in the mains, thus destabilizing the MGs.

Load changes in MGs can also aggravate frequency and voltage fluctuations. With an increase or decrease in the loads, the output power of the power generation unit cannot be suddenly changed. It takes time for a change to happen based on the supply and demand of sides to reach a new power balance point, and the quality of the output power will decline during the transient process.

These days, an ESS is installed to increase the inertia of the MGs. By detecting the frequency at PCC, ESS can provide the required active and reactive power support when the frequency decreases. Further, if the PCC frequency rises, the ESS will absorb the extra power to maintain the power balance of the system, which can alleviate the frequency-voltage fluctuations.

B. VSG Control Based on ESS

To provide inertial support through ESS, VSG is proposed to mimic the behavior of a synchronous generator [34], thus making the GCCs operate similarly to a traditional synchronous generator (SG) in terms of the operation mechanism and external characteristics.

The block diagram of a VSG control method is shown in Fig. 3. The "P-Droop" block is used to realize primary-frequency control; while the inertial equation in VSG is used as secondary-frequency control. Since the reactive power is mainly related to the PCC voltage, "Q-Droop" is used for output voltage control.

The "P-Droop" and "Q-Droop" equation of droop control method can be written as

$$\begin{cases} P = P_{ref} + m(\omega_{ref} - \omega_g) \\ E = E_{ref} + n(Q_{ref} - Q_e) \end{cases} \quad (3)$$

where m and n are the droop coefficients for frequency and reactive power, respectively; P_{ref}, Q_{ref}, E_{ref} and ω_{ref} are respectively the references of active power, reactive power, terminal voltage at PCC and angular speed of VSG; and ω_g and Q_e are the measured frequency and reactive power, respectively.

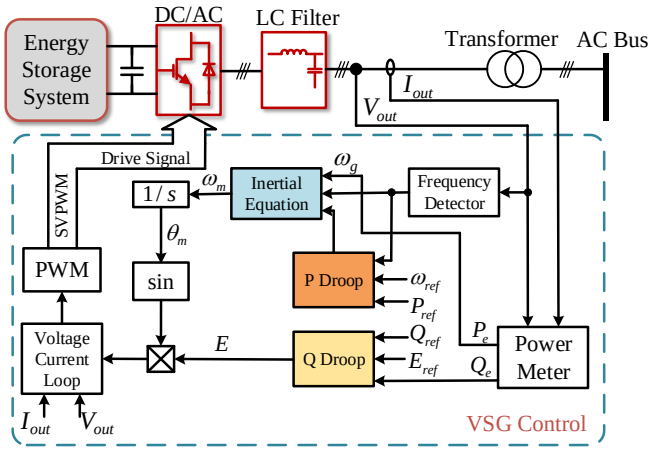

Fig. 3. Block diagram of the conventional VSG-ESS control method.

The inertial equation in VSG is given by

$$J\frac{d\omega_m}{dt} = \frac{P_m - P_e}{\omega_m} - D(\omega_m - \omega_0) \quad (4)$$

where J and D are the rotational inertia and damping coefficient, respectively; P_m and P_e are the mechanical and electromagnetic powers, respectively; and ω_m and ω_0 are the mechanical and rated angular frequencies, respectively.

Through the droop regulation of frequency and voltage, the power balance of the system can be guaranteed. However, during the regulation process, the frequency change can only be realized by simulating the rotor motion equation in (4). In cases when the load changes substantially, the frequency and voltage fluctuation may be very large, even to the point of pushing MGs into an unstable state. Therefore, it is vital to compensate the system through the ESS and suppress the frequency and voltage fluctuations.

Ⅲ. MPC-VSG Controller Design

The traditional VSG method involves controlling the voltage and frequency output through two droop links and an inertial simulation link of SG. In this method, if the system frequency fluctuates significantly, the regulation capability of VSG is limited. The rate-of-change-of-frequency (ROCOF) may be too large to be kept within the standard. Therefore, in this paper, MPC is introduced. As shown in Fig. 4, by detecting the changes in system frequency, and based on the system model, it is predicted to change the active and reactive power output $(\Delta P_{VSG}(k), \Delta Q_{VSG}(k))$ of VSG. As a result, the frequency regulation capability of VSG is enhanced.

In an island MGs, the power of multiple power converters needs to be regulated for parallel operation. To improve the power sharing and circulation suppression effect, it is necessary to add a virtual impedance in VSG control, as shown in Fig .4. Furthermore, the value of the virtual impedance will also affect the control effect of the VSG. This article refers to the methods in [35, 36] then selects a fixed virtual impedance Z_{VSG} for VSG control.

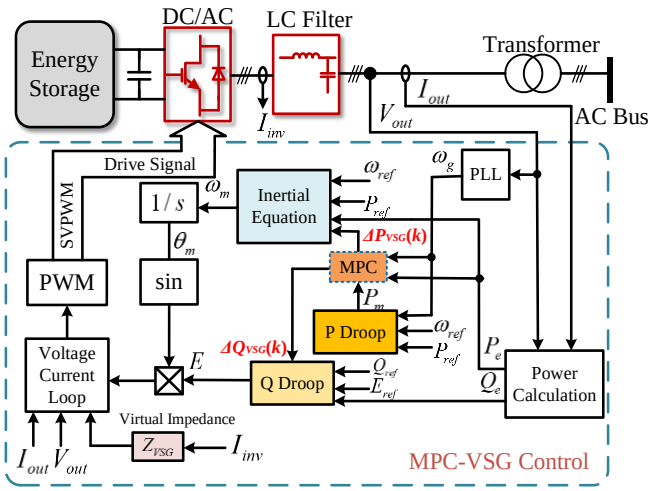

Fig. 4. Block diagram of the proposed MPC-VSG-ESS method.

A. Discrete MPC-VSG Control Method

To effectively realize frequency fluctuation suppression, the mathematical model of MPC-VSG needs to be first established.

According to (4), the inertial equation can be rewritten as the state-space model given by

$$\begin{cases} \dot{\omega}(t)=\frac{-D}{J}\omega(t)+\frac{1}{J\omega_m}P_m(t)-\frac{1}{J\omega_m}P_e(t) \\ y(t)=\omega(t) \end{cases} \tag{5}$$

where $\omega=\omega_m-\omega_0$. We may conclude from (5) that fluctuations in the output power of the RE can cause power imbalances both in the supply and demand sides, thus causing further frequency fluctuations. For VSG, the frequency fluctuation is small, and $\omega_m\approx\omega_0$ is approximated. The output power P_e can be regarded as the disturbance and P_m can be considered as the controllable input variable.

To realize (5) in digital implementation, after converting (5) into a discrete incremental model, the discrete state-equation can be derived as

$$\begin{cases} \Delta\omega(k+1)=\boldsymbol{A}\Delta\omega(k)+\boldsymbol{B_m}\Delta P_m(k)+\boldsymbol{B_e}\Delta P_e(k) \\ y(k+1)=\Delta\omega(k+1)+y(k) \end{cases} \tag{6}$$

where

$$\boldsymbol{A}=e^{-\frac{D}{J}T_s},\ \boldsymbol{B_m}=\frac{1}{J\omega_0}\int_0^{T_s}e^{-\frac{D}{J}\tau}d\tau,\ \boldsymbol{B_e}=-\frac{1}{J\omega_0}\int_0^{T_s}e^{-\frac{D}{J}\tau}d\tau \tag{7}$$

where T_s is the sampling time. The frequency, mechanical and electrical power variations can be written as

$$\begin{cases} \Delta\omega(k)=\omega(k)-\omega(k-1) \\ \Delta P_m(k)=P_m(k)-P_m(k-1) \\ \Delta P_e(k)=P_e(k)-P_e(k-1) \end{cases} \tag{8}$$

To improve the prediction accuracy and ensure that the required calculation expense is affordable, three-step prediction is selected as the prediction horizon. Therefore, the frequency prediction equation can be expressed as

$$\boldsymbol{Y_{p,c}}(k+1|k)=\boldsymbol{S}_A\Delta\omega(k)+\boldsymbol{I}y(k)+\boldsymbol{S_e}\Delta P_e(k)+\boldsymbol{S_m}\Delta P_m(k) \tag{9}$$

Where

$$\boldsymbol{S_A}=[\boldsymbol{A}\quad\sum_1^2\boldsymbol{A}^i\quad\sum_1^3\boldsymbol{A}^i]^T,\ \boldsymbol{I}=[1\quad 1\quad 1]^T$$

$$\boldsymbol{S_e}=[\boldsymbol{B_e}\quad\sum_1^2\boldsymbol{A}^{i-1}\boldsymbol{B_e}\quad\sum_1^3\boldsymbol{A}^{i-1}\boldsymbol{B_e}]^T$$

$$\boldsymbol{S_m}=\begin{bmatrix}\boldsymbol{B_m} & 0 & 0\\ \sum_1^2\boldsymbol{A}^{i-1}\boldsymbol{B_m} & \boldsymbol{B_m} & 0\\ \sum_1^3\boldsymbol{A}^{i-1}\boldsymbol{B_m} & \sum_1^2\boldsymbol{A}^{i-1}\boldsymbol{B_m} & \boldsymbol{B_m}\end{bmatrix} \tag{10}$$

B. Cost Function Design

The cost function considers the frequency deviation $\Delta\omega$ and the rated power variation ΔP_m of VSG. The weighted sum of squares should be the minimum value, which is expressed as

$$J_p=\sum_{i=1}^3[(\alpha\Delta\omega(k+i|k))^2+(\beta\Delta P_m(k+i|k))^2] \tag{11}$$

where α and β are the weight coefficients of frequency and power change, respectively. Further, $\Delta\omega(k+i|k)$ and $\Delta P_m(k+i|k)$ are the angular speed error and active power error at instant k, respectively. Since the frequency fluctuation should be limited within a certain range, the MPC optimization problem with constraints is described as:

$$\min_{\Delta P_m(k)} J_p(\Delta\omega(k),\Delta P_m(k)) \tag{12}$$

The cost function in (12) should satisfy the frequency constraints given as

$$\begin{cases} \Delta\omega(k+i+1|k)=\boldsymbol{A}\Delta\omega(k+i|k)+\boldsymbol{B_m}\Delta P_m(k+i|k)+\\ \qquad\qquad \boldsymbol{B_e}\Delta P_e(k+i|k) \\ \Delta\omega(k|k)=\Delta\omega(k) \\ y_c(k+i|k)=y_c(k+i-1|k)+\Delta\omega(k+i|k),i\geq 1 \\ y_c(k|k)=y_c(k) \\ y_{\min}(k)\leq y_c(k)\leq y_{\max}(k),\forall k\geq 0 \end{cases} \tag{13}$$

Then the cost function in (12) can be rewritten as

$$\begin{aligned} J_p(\Delta\omega(k),\Delta P_m(k))=&\|\boldsymbol{\Gamma_y}(\boldsymbol{Y_{p,c}}(k+1|k)-\boldsymbol{R}(k+1))\|^2\\ &+\|\boldsymbol{\Gamma_{P_m}}\boldsymbol{\Delta P_m}(k)\|^2 \end{aligned} \tag{14}$$

where $\boldsymbol{\Gamma_y}$ and $\boldsymbol{\Gamma_{P_m}}$ refer to the weighting coefficients matrix for angular frequency and active power error, and $\boldsymbol{R}(k+1)$ is the control output reference sequence at $k+1$. $\boldsymbol{\Gamma_y}$, $\boldsymbol{\Gamma_{P_m}}$ and $\boldsymbol{R}(k+1)$ can be respectively expressed as

$$\begin{cases} \boldsymbol{\Gamma_y}=\text{diag}\{\alpha,\alpha,\alpha\} \\ \boldsymbol{\Gamma_{P_m}}=\text{diag}\{\beta,\beta,\beta\} \\ \boldsymbol{R}(k+1)=[0\quad 0\quad 0]^T \end{cases} \tag{15}$$

where $\boldsymbol{\Delta P_m}(k)$ is a sequence of control quantity increments, which is used as an independent variable for the constrained optimization problem and defined as

$$\boldsymbol{\Delta P_m}(k)\overset{\text{def}}{=}\begin{bmatrix}\Delta P_m(k)\\ \Delta P_m(k+1)\\ \Delta P_m(k+2)\end{bmatrix} \tag{16}$$

Assume $\boldsymbol{Y_{p,c}}(k+1|k)$ is the three-step MPC control output at instant k, defined as

$$\boldsymbol{Y_{p,c}}(k+1|k) \overset{\text{def}}{=} \begin{bmatrix} y_c(k+1|k) \\ y_c(k+2|k) \\ y_c(k+3|k) \end{bmatrix} \tag{17}$$

In general, due to the existence of constraints, an analytical solution to the optimization problem in (12) cannot be obtained. Therefore, using the numerical solution method, the constrained MPC optimization problem is also a quadratic programming problem, so the optimization problem can be transformed into a quadratic programming (QP) description. Equation (14) can be transformed into a form of $\boldsymbol{z^T H z - g^T z}$, where $\boldsymbol{z = \Delta P_m}(k)$ is an independent variable of the optimization problem. Substituting (9) into the cost function in (14) and defining

$$\boldsymbol{E_p}(k+1|k) \overset{\text{def}}{=} \boldsymbol{R}(k+1) - \boldsymbol{S_A}\Delta\omega(k) - \boldsymbol{I}y(k) - \boldsymbol{S_e}\Delta P_e(k) \tag{18}$$

Then the cost function in (14) becomes

$$\begin{aligned} J_p =& \|\boldsymbol{\Gamma_y}(\boldsymbol{S_m}\boldsymbol{\Delta P_m}(k) - \boldsymbol{E_p}(k+1|k))\|^2 + \|\boldsymbol{\Gamma_{P_m}}\boldsymbol{\Delta P_m}(k)\|^2 \\ =& \boldsymbol{\Delta P_m}(k)^T \boldsymbol{S_m}^T \boldsymbol{\Gamma_y}^T \boldsymbol{\Gamma_y} \boldsymbol{S_m} \boldsymbol{\Delta P_m}(k) \\ &+ \boldsymbol{\Delta P_m}(k)^T \boldsymbol{\Gamma_{P_m}}^T \boldsymbol{\Gamma_{P_m}} \boldsymbol{\Delta P_m}(k) \\ &- 2\boldsymbol{E_p}(k+1|k)^T \boldsymbol{\Gamma_y}^T \boldsymbol{\Gamma_y} \boldsymbol{S_m} \boldsymbol{\Delta P_m}(k) \\ &+ \boldsymbol{E_p}(k+1|k)^T \boldsymbol{\Gamma_y}^T \boldsymbol{\Gamma_y} \boldsymbol{E_p}(k+1|k) \end{aligned} \tag{19}$$

Since $\boldsymbol{E_p}(k+1|k)^T \boldsymbol{\Gamma_y}^T \boldsymbol{\Gamma_y} \boldsymbol{E_p}(k+1|k)$ is independent of the variable $\boldsymbol{\Delta P_m}(k)$, equation (19) is equal to (20) shown as

$$J_p = \boldsymbol{\Delta P_m}(k)^T \boldsymbol{H} \boldsymbol{\Delta P_m}(k) - \boldsymbol{G}(k+1|k)^T \boldsymbol{\Delta P_m}(k) \tag{20}$$

Where

$$\begin{aligned} \boldsymbol{H} &= \boldsymbol{S_m}^T \boldsymbol{\Gamma_y}^T \boldsymbol{\Gamma_y} \boldsymbol{S_m} + \boldsymbol{\Gamma_{P_m}}^T \boldsymbol{\Gamma_{P_m}} \\ \boldsymbol{G}(k+1|k) &= 2\boldsymbol{S_m}^T \boldsymbol{\Gamma_y}^T \boldsymbol{\Gamma_y} \boldsymbol{E_p}(k+1|k) \end{aligned} \tag{21}$$

Then the frequency constraint in (13) is converted to the form of $\boldsymbol{Cz} \geq \boldsymbol{b}$, which can be described as

$$\boldsymbol{Y_{min}}(k+1) \leq \boldsymbol{Y_{p,c}}(k+1|k) \leq \boldsymbol{Y_{max}}(k+1) \tag{22}$$

Where

$$\begin{cases} \boldsymbol{Y_{min}}(k+1) = [y_{\min}(k+1) \quad y_{\min}(k+2) \quad y_{\min}(k+3)]^T \\ \boldsymbol{Y_{max}}(k+1) = [y_{\max}(k+1) \quad y_{\max}(k+2) \quad y_{\max}(k+3)]^T \end{cases} \tag{23}$$

Replacing (9) in (22), the frequency constraints can be converted to (24) as

$$\begin{bmatrix} -\boldsymbol{S_m} \\ \boldsymbol{S_m} \end{bmatrix} \boldsymbol{\Delta P_m}(k) \geq \boldsymbol{b}(k) \tag{24}$$

Where

$$\boldsymbol{b}(k) = \begin{bmatrix} \left(\boldsymbol{S_A}\Delta\omega(k) + \boldsymbol{I}y(k) + \boldsymbol{S_e}\Delta P_e(k)\right) - \boldsymbol{Y_{max}}(k+1) \\ -\left(\boldsymbol{S_A}\Delta\omega(k) + \boldsymbol{I}y(k) + \boldsymbol{S_e}\Delta P_e(k)\right) + \boldsymbol{Y_{min}}(k+1) \end{bmatrix} \tag{25}$$

Based on (24), the MPC optimization with constraints can be transformed into a QP problem described as

$$\begin{aligned} \min_{\Delta P_m(k)} \quad & \boldsymbol{\Delta P_m}(k)^T \boldsymbol{H} \boldsymbol{\Delta P_m}(k) - \boldsymbol{G}(k+1|k)^T \boldsymbol{\Delta P_m}(k) \\ \text{Satisfy}: \quad & \boldsymbol{C_m} \boldsymbol{\Delta P_m}(k) \geq \boldsymbol{b}(k) \end{aligned} \tag{26}$$

Where

$$\boldsymbol{C_m} = [-\boldsymbol{S_m} \quad \boldsymbol{S_m}]^T \tag{27}$$

Since $\boldsymbol{H} \geq 0$ in (21), the QP problem has a certain solution to any weighting matrix $\boldsymbol{\Gamma_y} \geq 0$, $\boldsymbol{\Gamma_{Pm}} \geq 0$, denoted as $\boldsymbol{\Delta P_m^*}(k)$. According to the operation principle of model predictive control, an initial control sequence will be imposed on the system. At the next sampling period, the constrained optimization problem will be updated, and the solution of (26) will be re-solved. After obtaining the optimal solution $\boldsymbol{\Delta P_m^*}$, the first term $\Delta P_m^*(k)$ in $\boldsymbol{\Delta P_m^*}$ is taken as the control quantity and re-input into the system. The variation of active power reference for VSG can be written as

$$\Delta P_{VSG}(k) = \Delta P_m^*(k) \tag{28}$$

From (2), it is known that the changes in active power will lead to changes in the PCC voltage. To reduce the voltage fluctuation, the reactive power of VSG should be changed accordingly. Further, the sum of the active and reactive power variations can be derived as

$$\begin{aligned} \Delta P_{VSG} + \Delta Q_{VSG} =& \frac{E\Delta V}{X}\sin\delta_0 + \frac{EV_0}{X}\cos\delta_0\Delta\delta \\ &+ \frac{E\Delta V}{X}\cos\delta_0 - \frac{2V_0\Delta V}{X} - \frac{EV_0}{X}\sin\delta_0\Delta\delta \end{aligned} \tag{29}$$

Considering $\delta_0 = 0$, (29) can be expressed as

$$\Delta P_{VSG} + \Delta Q_{VSG} = \frac{E\Delta V}{X} + \frac{EV_0}{X}\Delta\delta - \frac{2V_0\Delta V}{X} \tag{30}$$

To minimize the changes in ΔV, the mains voltage variation ΔV can be set as $\Delta V = 0$. The optimal $\Delta P_m^*(k)$ is the optimal active power that needs to be changed, and it is obtained through MPC. Thus, the voltage fluctuation can be minimized by setting the changes in reactive power as

$$\Delta Q_{VSG}(k) = -\Delta P_m^*(k) + \frac{EV_0}{X}\Delta\delta \tag{31}$$

By calculating the optimal active and reactive power ($\Delta P_{VSG}(k), \Delta Q_{VSG}(k)$), the reference power of VSG is constantly modified to achieve better dynamic responses in terms of both frequency and voltage. Fig. 5 shows the implementation of the proposed MPC-VSG controller.

C. Control Method Analysis

The control method needs to be discussed in two cases: one in which the solution of (26) is located inside the constraint boundary, and another in which the solution is located on the constraint boundary.

1) Solution to (26) is inside the constraint boundary

In this case, the model is degenerated into an unconstrained model. Assuming the optimal solution at this time is $\boldsymbol{\Delta P_m^*}(k)$.

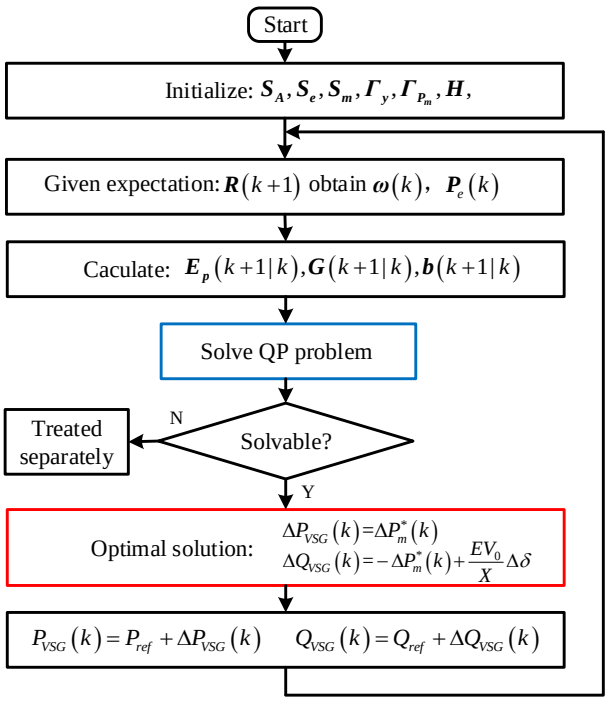

Fig. 5. Implementation of the proposed MPC-VSG controller.

$$\begin{aligned}\boldsymbol{\Delta P_m^*}(k) &= \boldsymbol{K_{mpc}}(\boldsymbol{R}(k+1) - \boldsymbol{S_A}\Delta\omega(k) - \boldsymbol{I}y(k) - \boldsymbol{S_e}\boldsymbol{\Delta P_e}(k)) \\ &= \boldsymbol{K_{mpc}}\boldsymbol{R}(k+1) - \boldsymbol{K_{mpc}}(\boldsymbol{S_A}+\boldsymbol{I})\Delta\omega(k) \\ &\quad -\boldsymbol{K_{mpc}}\boldsymbol{I}\omega(k-1) - \boldsymbol{K_{mpc}}\boldsymbol{S_e}\Delta P_e(k)\end{aligned} \tag{32}$$

Where

$$\boldsymbol{K_{mpc}}=(\boldsymbol{S_m}^T\boldsymbol{\Gamma_y}^T\boldsymbol{\Gamma_y}\boldsymbol{S_m}+\boldsymbol{\Gamma_{P_m}}^T\boldsymbol{\Gamma_{P_m}})^{-1}\boldsymbol{S_m}^T\boldsymbol{\Gamma_y}^T\boldsymbol{\Gamma_y} \tag{33}$$

Substituting $\Delta\boldsymbol{P_m}(k)$ in (32) into (6), the closed-loop control system can be derived as.

$$\begin{aligned}\Delta\omega(k+1) &= (\boldsymbol{A}-\boldsymbol{B_m}\boldsymbol{K_{mpc}}(\boldsymbol{S_A}+\boldsymbol{I}))\Delta\omega(k) \\ &\quad +\boldsymbol{B_u}\boldsymbol{K_{mpc}}\boldsymbol{R}(k+1) \\ &\quad +(\boldsymbol{B_e}-\boldsymbol{B_m}\boldsymbol{K_{mpc}}\boldsymbol{S_e})\Delta P_e(k) \\ &\quad -\boldsymbol{B_m}\boldsymbol{K_{mpc}}\boldsymbol{I}\omega(k-1)\end{aligned} \tag{34}$$

Obviously, if all the eigenvalues of $\boldsymbol{A}-\boldsymbol{B_m}\boldsymbol{K_{mpc}}(\boldsymbol{S_A}+\boldsymbol{I})$ are within the unit circle, the closed-loop system in (33) is nominally asymptotically stable.

$$|\boldsymbol{A}-\boldsymbol{B_m}\boldsymbol{K_{mpc}}(\boldsymbol{S_A}+\boldsymbol{I})|<1 \tag{35}$$

When inequation constraint (35) is satisfied, the system is stable. Therefore, after designing the system control parameters, they need to be verified based on the inequality in (35).

2) Solution to (26) is on the boundary of the feasible domain

In this case, the MPC will output the power according to its maximum value. The frequency adjustment will mainly be performed by other devices, and the frequency stability will mainly be determined by other devices.

In summary, the MPC-VSG control method can keep the system frequency stable within the limits. When it exceeds the range in which VSG can adjust, the MPC-VSG can also output its maximum value, keeping the system as stable as possible.

Ⅳ. Simulation Results

A. Simulation Setup

To verify the effectiveness of the proposed method, a MATLAB/Simulink model is set up and tested. Tables I shows the parameters of the diesel synchronous generator. In order to show the power compensation effect of the proposed method more clearly, the output power waveform is processed by a low-pass filter (LPF) with a cut-off frequency of 100 Hz. Before verifying the performance of the proposed method under different conditions, the appropriate inertia and damping coefficients need to be selected. The effects of different inertia and damping coefficients on a frequency transient are shown in Fig. 6. A set of appropriate inertia and damping coefficients are selected for the proposed method. After comparing different coefficients on frequency fluctuation suppression, the selected coefficients are presented in Table II.

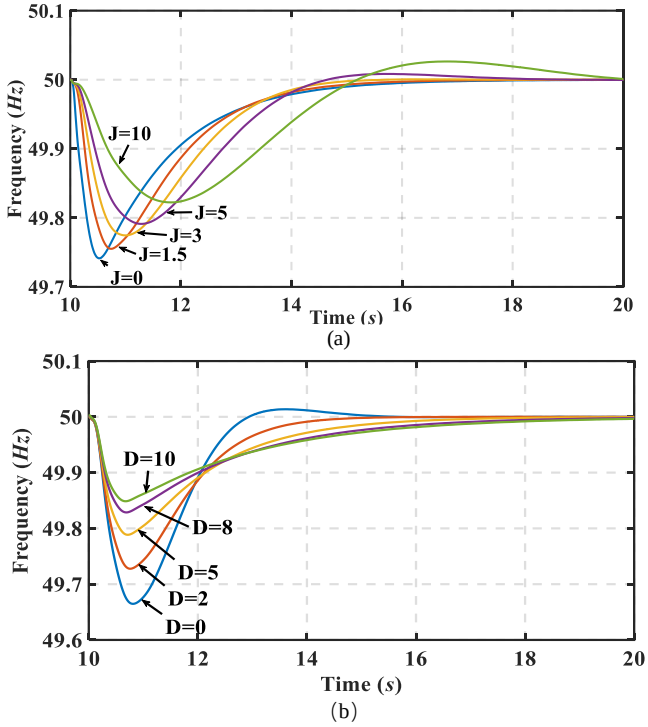

Fig. 6. Effects of the inertia and damping coefficients on mains frequency. (a) Different virtual inertia J ($D=2$); (b) Different virtual damping D ($J=1.5$).

B. Case 1: Comparisons of Different Control Method

To compare the voltage and frequency fluctuations with loading transitions, a 5 kW load is connected at $t = 8$ s and disconnected at $t = 16\,s$. Different working states are examined for comparison purposes. The "No-ESS" line indicates that the load is powered by the diesel synchronous generator. The "VSG-ESS" line represents the case in which an ESS controlled by the traditional VSG method is parallel-connected with SG to power the load. The "MPCVSG-ESS" line represents the case in which an ESS controlled by the MPC-VSG method is parallel-connected with SG to power the load.

TABLE I
DIESEL SYNCHRONOUS GENERATOR PARAMETERS

Parameter	Symbol	Value
Nominal power	P_{SG}	20 kVA
Nominal voltage (line to line)	V_n	380 V_{rms}
Nominal frequency	f_{SG}	50 Hz
Inertia coefficient	J_{SG}	0.6 kg · m^2
Damping coefficient	D_{SG}	0
Number of pole pairs	N	1

TABLE Ⅱ
PARAMETER SPECIFICATIONS IN VSG

Parameter	Symbol	Value
Nominal power	P_{VSG}	0 kVA
Nominal voltage (line to line)	u_{AB}, u_{BC}, u_{CA}	380 V_{rms}
DC-link voltage	U_{dc}	800 V
Nominal frequency of VSG	f_{VSG}	50 Hz
Virtual inertia	J_{VSG}	1.5 kg · m^2
Virtual damping	D_{VSG}	3.2
Virtual impedance	Z_{VSG}	0.5 + j0.004 Ω
P droop coefficient	m	1.5×10^{-4}
Q droop coefficient	n	2.2×10^{-4}
Switching frequency	f_{SW}	5 kHz

Fig.7 shows the power outputs of SG and ESS under No-ESS, with VSG-ESS, and with MPCVSG-ESS, respectively. In the case of ESS, as shown in Fig. 7(a), when the load changes, the output of SG changes immediately. ESS can provide extra power for the step-up load, as shown in Fig.7 (b), so that the output power of SG can change slowly. With the proposed method, ESS outputs more power when the load changes, which allows for smooth power output changes of SG.

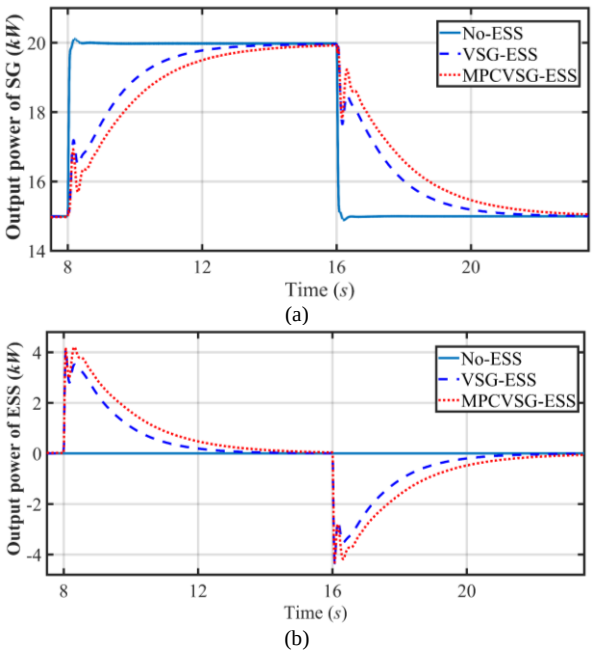

Fig. 7. Power output of SG and ESS during loading transitions. (a)Output of SG; (b) Output of ESS.

Fig.8 shows the frequency and ROCOF under loading transitions. From Fig. 8(a), the frequency variations of PCC are about 0.68, 0.19 and 0.25 Hz with the NO-ESS, MPC-VSG and MPCVSG-ESS method, respectively. The frequency variation has decreased by about 24%, which clearly improves the power quality and enhance the system stability. Compared with the capacity of MGs, the loading variation is low. Therefore, the frequency variation is also very low, which should not exceed ISO 8528-5 standard for the generator limit (±1.5 Hz).

Along with frequency changes, the ROCOF is also worthy of attention. As shown in Fig. 8(b). Before adding the ESS, the maximum ROCOF is about 2.27 Hz/s. The maximum ROCOF of the traditional VSG method is about 0.74 Hz/s, which does not meet the standard, i.e. ROCOF ≤ 0.6 Hz/s. It should also be noted that the maximum ROCOF with the proposed method is about 0.58 Hz/s, which represents a decrease of about 22% and satisfies the requirements of the ISO standard.

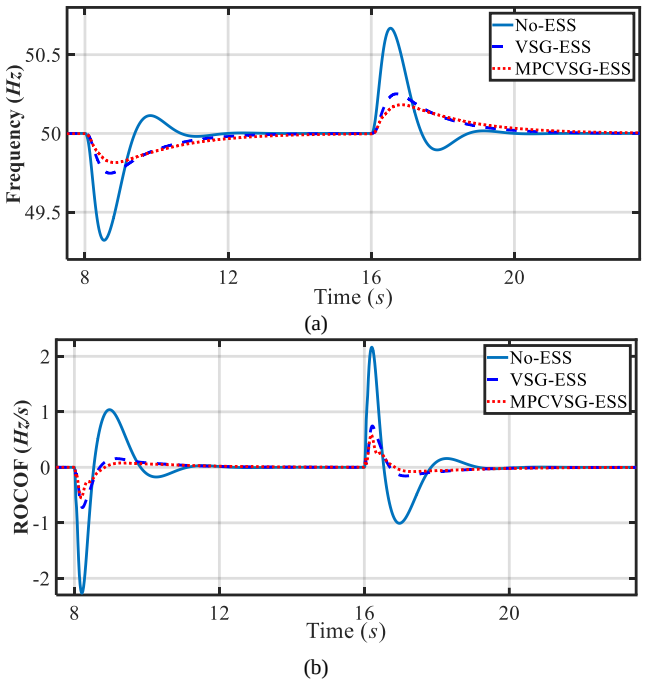

Fig. 8. Frequency and ROCOF under loading transitions. (a) Frequency changes; (b) ROCOF.

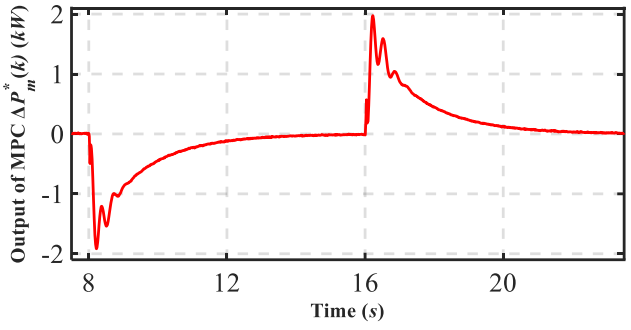

Fig. 9. Output power of MPC controller.

Fig. 9 shows the output power of the MPC. When the frequency changes, the MPC controller calculates the power changes caused by the frequency changes. For example, when a step-up load is given at $t = 8$ s, the frequency decreases. By detecting the frequency changes, the MPC calculates the required power change within a limited range. Then, MPC

outputs the optimized active power variations $\Delta P_m^*(k)$. By subtracting $\Delta P^*{}_{\mathrm{m}}(k)$, the rated power of VSG can be regulated adaptively.

After obtaining the optimized change in active power, the change in reactive power can be obtained by (31). By controlling the reactive power reference with the MPC-VSG method, the voltage fluctuation can be suppressed. The PCC voltage in Fig. 10 shows that, before the addition of the ESS, the voltage fluctuation is about -4.3 V when the load is connected, while it is 4.2 V when the loading is disconnected. When the traditional VSG-ESS is applied, the voltage fluctuation increases about -5.6 V when loading is connected and increases 5.6 V when loading is disconnected. With the proposed MPCVSG-ESS method, the voltage fluctuation decreases to -4.5 V when the load is connected and increases to 4.6 V when the load is disconnected. In both cases, the proposed method can reduce the voltage variations by 19.6% and 17.9%, respectively.

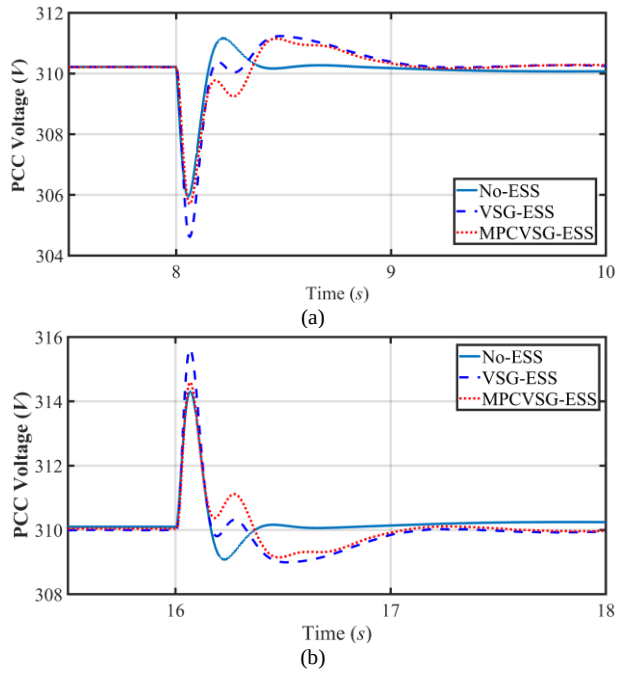

Fig. 10. PCC Voltage under loading transitions. (a) Loading connected; (b) Loading disconnected.

The above simulation results prove that the MPC-VSG control method can improve the power quality and reduce the voltage and frequency fluctuations under loading transitions, which verifies the effectiveness of the proposed method.

C. Case 2 : Power Sharing Performances to Load Change

To verify the adaptability of the proposed method to the island MGs, two VSGs are connected in parallel to power the loads. The main parameters of the two VSGs are the same as those in Table II, and the different parts are shown in Table III. Before 2 s, VSG1 and VSG2 are connected in parallel to power the 15 kW load. At 2 s, another 15 kW load is connected, and which is disconnected at 12 s.

TABLE III
DIESEL SYNCHRONOUS GENERATOR PARAMETERS

Parameter	Symbol	Value
Nominal power	P_{VSG1}, P_{VSG2}	20 kVA, 10 kVA
Virtual inertia	J_{VSG1}, J_{VSG2}	0.1 kg · m^2, 0.05 kg · m^2
Virtual damping	D_{VSG1}, D_{VSG2}	8, 4
P droop coefficient	m_{VSG1}, m_{VSG2}	2.5×10^{-5}, 5×10^{-5}
Q droop coefficient	n_{VSG1}, n_{VSG2}	4.4×10^{-5}, 2.2×10^{-4}
Load power	P_{L1}, P_{L2}	15 kW
Virtual impedance	Z_{VSG1}, Z_{VSG2}	0.8 + j0.006 Ω

As shown in Fig. 11, before t = 2 s, VSG1 and VSG2 are connected in parallel to power the load, and the ratio of output power is the same as rated power, which is 2:1. When the additional load with 15 kW is connected, VSG1 and VSG2 can increase their power output at the same time. Similarly, when the load is removed at 12 s, they can also scale down their output at the same proportion. At steady state, the output continues to be maintained at the same ratio.

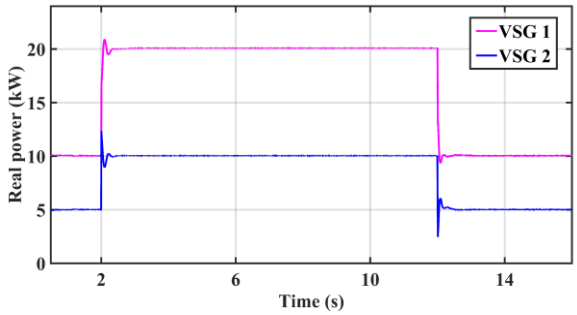

Fig. 11. Real power of ESS under loading transitions.

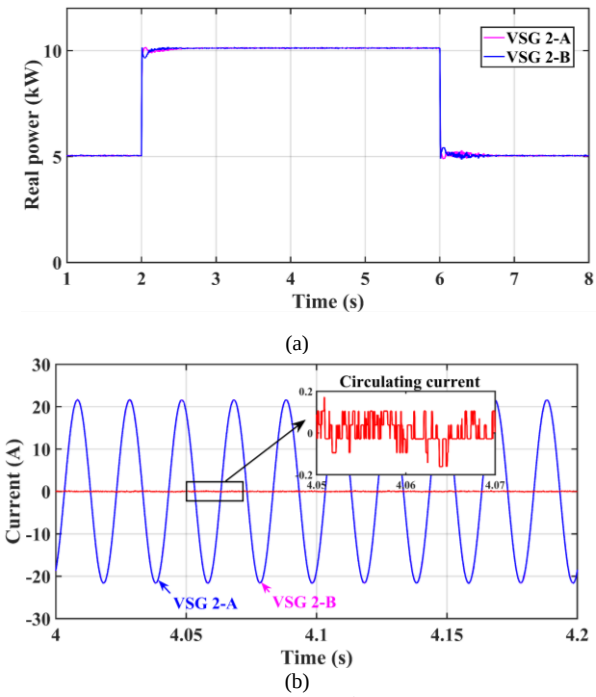

Fig. 12. The real power and current outputs of parallel connected VSG2-A and VSG2-B under loading transitions. (a) Real power; (b) Output current and circulating current.

Fig. 12 shows the parallel operation of two VSGs with the same parameters as VSG2, denoted as VSG2-A and VSG2-B, respectively. Before 2 s, VSG2-A and VSG2-B are connected in parallel to power a 10 kW load. At 2 s, another 10 kW load is connected to the system, they each share the load power by 5 kW. With the removal of the extra load at 6 s, the output power is each recovered to 5 kW. From Fig.12 (a), it can be seen that VSG2-A and VSG2-B have the same power outputs under loading transitions. The steady-state output currents of VSG2-A and VSG2-B are shown in Fig.12 (b). The output currents of the two VSGs are basically the same, and the circulating current is less than 0.1 A.

From all the above simulation results, the proposed method has the capabilities of not only voltage and frequency fluctuations mitigation, but also the power sharing and circulating current suppression . The proposed MPC-VSG ESS can accurately and proportionally output its power in parallel connection, which further proves the its applicability in MGs.

V . Experimental Results

A. Hardware Setup

To further validate the aforementioned study, experimental verifications are performed. Due to the parallel operation complexity involved with the multiple power converters, loads, ESS, and SG, a Hardware-In-Loop (HIL) test is used, as it can offer the most complex model-based design for interacting with real-world environments.

In the experiment, RT-LAB (OP4050) was used as the Real-Time Simulator for power stage emulation. Similarly, MicroLabBox which is a compact, versatile, and powerful development system for laboratory tests, was used for NO-ESS, VSG-ESS, and MPC-VSG-ESS control realization. Fig. 13 shows the experimental setup. The modelings of loads, switching devices, driving circuits, SG and ESS are all set up in RT-LAB. MicroLabBox samples the output signals of RT-LAB (e.g. grid current, voltage, frequency, active and reactive powers, etc.). The control signal is generated according to the proposed method then sent back to RT-LAB. The sampling time is 40 μs. As a result, a closed-loop emulation platform for MGs is established.

The HIL tests are mainly performed for two purposes: 1) the correctness and effectiveness of the MPC-VSG-ESS are validated in utility; 2) the accuracy and real-time computational ability of the MPC-VSG based ESS system are evaluated.

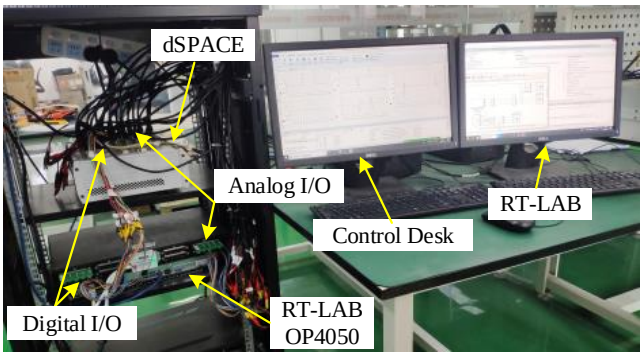

Fig. 13. Configuration of HIL experimental platform.

B. Results and Analysis

The experimental results are shown in Figs. 14, 15, and 16. Compared with the aforementioned simulation results, the experiment results are very similar, but there is some deviation.

1) Performance of SG with and without ESS

Fig. 14 shows the output power of SG and ESS under load transitions without ESS, with VSG-ESS, and with MPCVSG-ESS, respectively. The results show that the waveform of the experimental results is similar to the simulation results, and that the proposed MPCVSG-ESS method could greatly alleviate the output power of SG.

2) Grid Voltage and Frequency Regulation Capability

Fig. 15 shows the dynamic performance of the PCC frequency variations with No-ESS, VSG-ESS, and MPCVSG-ESS under load transitions, respectively. The load is connected at $t = 30$ s and disconnected at $t = 40$ s. When only SG is operated in MGs, the frequency fluctuation is about 0.64 Hz, while the ROCOF is about 1.64 Hz/s. With the traditional VSG method, the frequency fluctuation is reduced to 0.22 Hz while the ROCOF is reduced to 0.34 Hz/s. When the ESS is controlled by the MPC-VSG method, the frequency variation is only 0.16 Hz, and the ROCOF decreases to 0.23Hz/s. The comparison results indicate that the proposed method can effectively suppress frequency fluctuations, thus enhancing the frequency dynamic performance of the system.

Fig. 16 shows the PCC voltage variations when the load is connected at t = 30 s and disconnected at t = 40 s. When only SG is operated, the voltage drop is about 5.2 V when the load is connected, and the voltage-rise is about 4.7 V when the load is disconnected. When traditional VSG-ESS is applied, the voltage-overshoot is about 7 V. For the MPCVSG-ESS method, the voltage overshoot is about 5.6 V when a cut-in load is connected, and it is about 4.8 V when the load is disconnected.

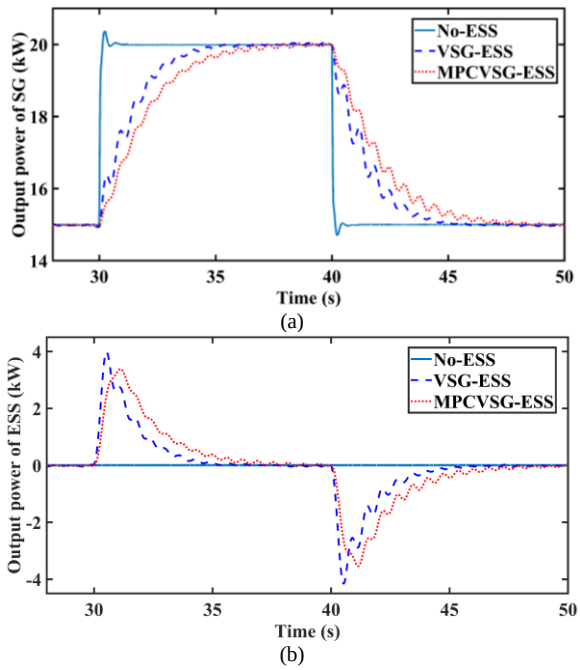

Fig. 14. Output power of ESS under loading transitions. (a) Output of SG; (b) Output of ESS.

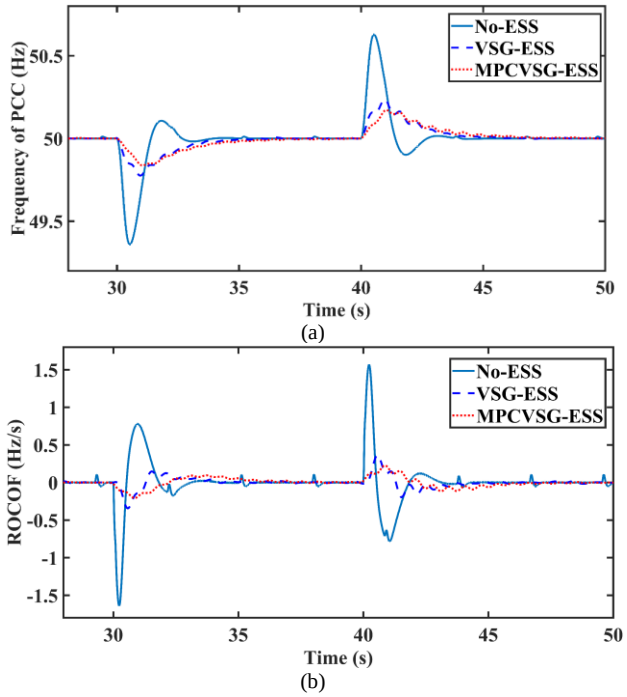

Fig. 15. Frequency fluctuations of PCC under loading transition. (a) Frequency changes of PCC; (b) ROCOF of PCC.

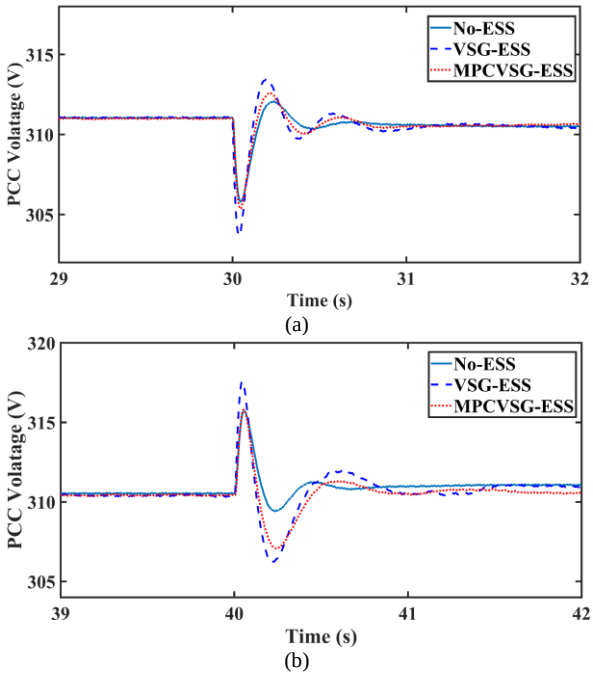

Fig. 16. Voltage fluctuations of PCC under loading transition. (a) Loading connected; (b) Loading disconnected.

Based on the results shown in Figs. 14, 15, and 16, it can be concluded that the proposed method reduces not only the frequency fluctuation but also the voltage fluctuations.

VI. Conclusions

This paper investigates a three-step prediction MPC-VSG control method for an ESS in islanded MGs. Based on the real-time detection of the system frequency, the mathematical model of a VSG is established to predict the optimal output power of VSG, thereby further enhancing the frequency dynamics of the system. In addition, considering that changes in active power may lead to voltage variation, we proposed a voltage suppression method that can reduce the voltage fluctuation by changing the rated reactive power of VSG. The HIL platform was used to implement the proposed control method and to verify the simulation results. Numerous simulation and experimental results have demonstrated that the dynamic performance of the frequency and voltage of the mains in MG under load changes can be enhanced, and the correctness and effectiveness of the proposed method in this study have been verified. It is suggested that future works on the frequency and voltage fluctuation suppression of MGs can focus on combing neural networks with the MPC-VSG method.

References

[1] X. S. Tang, X. Hu, N. N. Li, W. Deng, and G. W. Zhang, "A Novel Frequency and Voltage Control Method for Islanded Microgrid Based on Multienergy Storages," *IEEE Transactions on Smart Grid*, Article vol. 7, no. 1, pp. 410-419, Jan 2016.

[2] D. E. Olivares *et al.*, "Trends in Microgrid Control," *IEEE Transactions on Smart Grid*, vol. 5, no. 4, pp. 1905-1919, 2014.

[3] D. Wu, F. Tang, T. Dragicevic, J. C. Vasquez, and J. M. Guerrero, "A Control Architecture to Coordinate Renewable Energy Sources and Energy Storage Systems in Islanded Microgrids," *IEEE Transactions on Smart Grid*, Article vol. 6, no. 3, pp. 1156-1166, May 2015.

[4] J. W. Simpson-Porco, Q. Shafiee, F. Dorfler, J. C. Vasquez, J. M. Guerrero, and F. Bullo, "Secondary Frequency and Voltage Control of Islanded Microgrids via Distributed Averaging," *IEEE Transactions on Industrial Electronics*, Article vol. 62, no. 11, pp. 7025-7038, Nov 2015.

[5] V. Nasirian, S. Moayedi, A. Davoudi, and F. L. Lewis, "Distributed Cooperative Control of DC Microgrids," *IEEE Transactions on Power Electronics*, vol. 30, no. 4, pp. 2288-2303, 2015.

[6] N. M. Dehkordi, N. Sadati, and M. Hamzeh, "Fully Distributed Cooperative Secondary Frequency and Voltage Control of Islanded Microgrids," *IEEE Transactions on Energy Conversion*, vol. 32, no. 2, pp. 675-685, 2017.

[7] H. Wu *et al.*, "Small-Signal Modeling and Parameters Design for Virtual Synchronous Generators," *IEEE Transactions on Industrial Electronics*, Article vol. 63, no. 7, pp. 4292-4303, Jul 2016.

[8] Q. Zhong and G. Weiss, "Synchronverters: Inverters That Mimic Synchronous Generators," *IEEE Transactions on Industrial Electronics*, vol. 58, no. 4, pp. 1259-1267, 2011.

[9] J. Liu, Y. Miura, and T. Ise, "Comparison of Dynamic Characteristics Between Virtual Synchronous Generator and Droop Control in Inverter-Based Distributed Generators," *IEEE Transactions on Power Electronics*, Article vol. 31, no. 5, pp. 3600-3611, May 2016.

[10] J. Alipoor, Y. Miura, and T. Ise, "Power System Stabilization Using Virtual Synchronous Generator With Alternating Moment of Inertia," *IEEE Journal of Emerging and Selected Topics in Power Electronics*, Article vol. 3, no. 2, pp. 451-458, Jun 2015.

[11] S. D'Arco, J. A. Suul, and O. B. Fosso, "Small-signal modeling and parametric sensitivity of a virtual synchronous machine in islanded operation," *International Journal of Electrical Power & Energy Systems*, vol. 72, pp. 3-15, 2015.

[12] H. Wu *et al.*, "Small-Signal Modeling and Parameters Design for Virtual Synchronous Generators," *IEEE Transactions on Industrial Electronics*, vol. 63, no. 7, pp. 4292-4303, 2016.

[13] T. Shintai, Y. Miura, and T. Ise, "Oscillation Damping of a Distributed Generator Using a Virtual Synchronous Generator," *IEEE Transactions on Power Delivery*, vol. 29, no. 2, pp. 668-676, 2014.

[14] D. D. Li, Q. W. Zhu, S. F. Lin, and X. Y. Bian, "A Self-Adaptive Inertia and Damping Combination Control of VSG to Support Frequency Stability," *IEEE Transactions on Energy Conversion*, Letter vol. 32, no. 1, pp. 397-398, Mar 2017.

[15] Y. Hirase, K. Abe, K. Sugimoto, K. Sakimoto, H. Bevrani, and T. Ise, "A novel control approach for virtual synchronous generators to suppress

frequency and voltage fluctuations in microgrids," *Applied Energy,* Article vol. 210, pp. 699-710, Jan 2018.
[16] N. Mendis, K. M. Muttaqi, and S. Perera, "Management of Low- and High-Frequency Power Components in Demand-Generation Fluctuations of a DFIG-Based Wind-Dominated RAPS System Using Hybrid Energy Storage," *IEEE Transactions on Industry Applications,* Article vol. 50, no. 3, pp. 2258-2268, May-Jun 2014.
[17] A. M. Howlader, N. Urasaki, A. Yona, T. Senjyu, and A. Y. Saber, "A review of output power smoothing methods for wind energy conversion systems," *Renewable & Sustainable Energy Reviews,* Review vol. 26, pp. 135-146, Oct 2013.
[18] Q. Y. Jiang, Y. Z. Gong, and H. J. Wang, "A Battery Energy Storage System Dual-Layer Control Strategy for Mitigating Wind Farm Fluctuations," *IEEE Transactions on Power Systems,* Article vol. 28, no. 3, pp. 3263-3273, Aug 2013.
[19] J. L. Domínguez-García, O. Gomis-Bellmunt, F. D. Bianchi, and A. Sumper, "Power oscillation damping supported by wind power: A review," *Renewable and Sustainable Energy Reviews,* vol. 16, no. 7, pp. 4994-5006, 2012.
[20] A. Pratap, Z. Ziadi, N. Urasaki, and T. Senjyu, "Smoothing of Wind Power Fluctuations for Permanent Magnet Synchronous Generator-Based Wind Energy Conversion System and Fault Ride-through Consideration," *Electric Power Components and Systems,* Article vol. 43, no. 3, pp. 271-281, Feb 2015.
[21] S. Shivashankar, S. Mekhilef, H. Mokhlis, and M. Karimi, "Mitigating methods of power fluctuation of photovoltaic (PV) sources - A review," *Renewable & Sustainable Energy Reviews,* Review vol. 59, pp. 1170-1184, Jun 2016.
[22] J. Rocabert, A. Luna, F. Blaabjerg, and P. Rodríguez, "Control of Power Converters in AC Microgrids," *IEEE Transactions on Power Electronics,* vol. 27, no. 11, pp. 4734-4749, 2012.
[23] F. Garcia-Torres and C. Bordons, "Optimal Economical Schedule of Hydrogen-Based Microgrids With Hybrid Storage Using Model Predictive Control," *IEEE Transactions on Industrial Electronics,* Article vol. 62, no. 8, pp. 5195-5207, Aug 2015.
[24] T. I. Bo and T. A. Johansen, "Battery Power Smoothing Control in a Marine Electric Power Plant Using Nonlinear Model Predictive Control," *IEEE Transactions on Control Systems Technology,* Article vol. 25, no. 4, pp. 1449-1456, Jul 2017.
[25] A. Di Giorgio, F. Liberati, A. Lanna, A. Pietrabissa, and F. D. Priscoli, "Model Predictive Control of Energy Storage Systems for Power Tracking and Shaving in Distribution Grids," *IEEE Transactions on Sustainable Energy,* Article vol. 8, no. 2, pp. 496-504, Apr 2017.
[26] J. Pahasa and I. Ngamroo, "Coordinated Control of Wind Turbine Blade Pitch Angle and PHEVs Using MPCs for Load Frequency Control of Microgrid," *IEEE Systems Journal,* Article vol. 10, no. 1, pp. 97-105, Mar 2016.
[27] M. H. Khooban, T. Dragicevic, F. Blaabjerg, and M. Delimar, "Shipboard Microgrids: A Novel Approach to Load Frequency Control," *IEEE Transactions on Sustainable Energy,* Article vol. 9, no. 2, pp. 843-852, Apr 2018.
[28] H. Bevrani, M. R. Feizi, and S. Ataee, "Robust Frequency Control in an Islanded Microgrid: H-infinity and mu-Synthesis Approaches," *IEEE Transactions on Smart Grid,* Article vol. 7, no. 2, pp. 706-717, Mar 2016.
[29] M. H. Khooban, T. Niknam, F. Blaabjerg, and T. Dragievic, "A new load frequency control strategy for micro-grids with considering electrical vehicles," *Electric Power Systems Research,* Article vol. 143, pp. 585-598, Feb 2017.
[30] Y. Mi, Y. Fu, D. D. Li, C. S. Wang, P. C. Loh, and P. Wang, "The sliding mode load frequency control for hybrid power system based on disturbance observer," *International Journal of Electrical Power & Energy Systems,* Article vol. 74, pp. 446-452, Jan 2016.
[31] T. B. Yang, K. T. Mok, S. C. Tan, C. K. Lee, and S. Y. Hui, "Electric Springs With Coordinated Battery Management for Reducing Voltage and Frequency Fluctuations in Microgrids," *IEEE Transactions on Smart Grid,* Article vol. 9, no. 3, pp. 1943-1952, May 2018.
[32] A. D. Paquette, M. J. Reno, R. G. Harley, and D. M. Divan, "Sharing Transient Loads : Causes of Unequal Transient Load Sharing in Islanded Microgrid Operation," *IEEE Industry Applications Magazine,* vol. 20, no. 2, pp. 23-34, 2014.
[33] Z. Y. Wang, B. K. Chen, J. H. Wang, and J. Kim, "Decentralized Energy Management System for Networked Microgrids in Grid-Connected and Islanded Modes," *IEEE Transactions on Smart Grid,* Article vol. 7, no. 2, pp. 1097-1105, Mar 2016.
[34] J. Y. Fang, Y. Tang, H. C. Li, and X. Q. Li, "A Battery/Ultracapacitor Hybrid Energy Storage System for Implementing the Power Management of Virtual Synchronous Generators," *IEEE Transactions on Power Electronics,* Article vol. 33, no. 4, pp. 2820-2824, Apr 2018.
[35] A. D. Paquette and D. M. Divan, "Virtual Impedance Current Limiting for Inverters in Microgrids With Synchronous Generators," *IEEE Transactions on Industry Applications,* Article vol. 51, no. 2, pp. 1630-1638, Mar-Apr 2015.
[36] R. J. Wai, Q. Q. Zhang, and Y. Wang, "A Novel Voltage Stabilization and Power Sharing Control Method Based on Virtual Complex Impedance for an Off-Grid Microgrid," *IEEE Transactions on Power Electronics,* Article vol. 34, no. 2, pp. 1863-1880, Feb 2019.

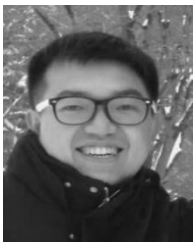

BO Long (S'08–M'10) received the B.S. degree in electrical engineering from the Xi'an Petroleum University, Xian, China, in 2001, and the Ph.D. degree in electrical engineering from Xian Jiaotong University, Shanxi, China, in 2008. He joined the Department of Power Electronics, School of Mechatronics Engineering, UESTC, in 2008, and has been promoted to an Associate Professor since 2014. From 2017 to 2018, he was a Visiting Scholar (Guest Post-Doctoral Researcher) in the area of renewable energy and microgrids with the Department of Electrical Engineering, Tsinghua University, Beijing, China. His research interests include ac/dc microgrids, grid-connected converters for renewable energy systems and DGs, model predictive control, power quality, multilevel converters, ac motor control, and resonance suppression technique for smart grid applications. He has authored over 20 SCIE-indexed journal papers and one book chapter in the area of power electronics, motor control, battery management system, and smart grid. He has seven issued and 10 pending patents. He is currently the supervisor for eleven master students, two of which have been nominated as provincial outstanding graduate student of UESTC. He is an active Reviewer for the IEEE TRANSACTIONS ON POWER ELECTRONICS, ISA TRANSACTIONS, APPLIED ENERGY, ENERGY, the IEEE TRANSACTIONS ON SMART GRID, the IEEE TRANSACTIONS ON I NDUSTRIAL ELECTRONICS, the IEEE TRANSACTIONS ON SUSTAINABLE ENERGY, and the IEEE TRANSACTIONS ON ENERGY CONVERSION.

Yong Liao received the B.S. degree in mechanical engineering from Southeast University, Nanjing, China, in 2017. He is currently pursuing the M.S. degree in mechanical engineering from University of Electronic Science and Technology of China, Chengdu, China. His current research interests include the optimization of ac microgrids, power distribution. Specifically, research on the method of using model predictive control technology to optimize the traditional inverter control system.

Kil To Chong received the Ph.D. degree in mechanical engineering from Texas A&M University, in 1995. He is currently a Professor and the Department Head of the School of Electronics and Information Engineering and a member and the Head of the Advanced Electronics and Information Research Center, Chonbuk National University, Jeonju, South Korea. His research interests include motor fault detection and control, network system control, sensor network systems, time-delay systems, and neural networks

José Rodríguez (M'81-SM'94-F'10) received the Engineer degree in electrical engineering from the Universidad Tecnica Federico Santa Maria, in Valparaiso, Chile, in 1977 and the Dr.-Ing. degree in electrical engineering from the University of Erlangen, Erlangen, Germany, in 1985. He has been with the Department of Electronics Engineering, Universidad Tecnica Federico Santa Maria, since 1977, where he was a full professor and President. Since 2015 he is the President of Universidad Andres Bello in Santiago, Chile. He has co-authored two books, several book chapters, and more than 400 journal and conference papers. His main research interests include multilevel inverters, new converter topologies, control of power converters, and adjustable-speed drives. He has received a number of best paper awards from journals of the IEEE. Dr. Rodriguez is a member of the Chilean Academy of Engineering. In 2014 he received the National Award of Applied Sciences and Technology from the government of Chile. In 2015, he received the Eugene Mittelmann Award from the Industrial Electronics Society of the IEEE.

Josep M. Guerrero (S'01-M'04-SM'08-FM'15) received the B.S. degree in telecommunications engineering, the M.S. degree in electronics engineering, and the Ph.D. degree in power electronics from the Technical University of Catalonia, Barcelona, in 1997, 2000 and 2003, respectively. Since 2011, he has been a Full Professor with the Department of Energy Technology, Aalborg University, Denmark, where he is responsible for the Microgrid Research Program. From 2014 he is chair Professor in Shandong University; from 2015 he is a distinguished guest Professor in Hunan University; and from 2016 he is a visiting professor fellow at Aston University, UK, and a guest Professor at the Nanjing University of Posts and Telecommunications. From 2019, he became a Villum Investigator by The Villum Fonden, which supports the Center for Research on Microgrids (CROM) at Aalborg University, being Prof. Guerrero the founder and Director of the same center (www.crom.et.aau.dk). His research interests are oriented to different microgrid aspects, including power electronics, distributed energy-storage systems, hierarchical and cooperative control, energy management systems, smart metering and the internet of things for AC/DC microgrid clusters and islanded microgrids. Specially focused on microgrid technologies applied to offshore wind, maritime microgrids for electrical ships, vessels, ferries and seaports, and space microgrids applied to nanosatellites and spacecrafts. Prof. Guerrero is an Associate Editor for a number of IEEE TRANSACTIONS. He has published more than 600 journal papers in the fields of microgrids and renewable energy systems, which are cited more than 50,000 times. He received the best paper award of the IEEE Transactions on Energy Conversion for the period 2014-2015, and the best paper prize of IEEE-PES in 2015. As well, he received the best paper award of the Journal of Power Electronics in 2016. During six consecutive years, from 2014 to 2019, he was awarded by Clarivate Analytics (former Thomson Reuters) as Highly Cited Researcher with 50 highly cited papers. In 2015 he was elevated as IEEE Fellow for his contributions on "distributed power systems and microgrids."